Edges in models of shear flow

Norman Lebovitz[1],† and Giulio Mariotti[2]

[1]Department of Mathematics, University of Chicago, 5734 S University Ave, Chicago, IL 60637, USA

[2]Department of Earth, Atmospheric and Planetary Sciences, Massachusetts Institute of Technology, 77 Massachusetts Ave, Cambridge, MA 02139, USA

A characteristic feature of the onset of turbulence in shear flows is the appearance of an 'edge', a codimension-one invariant manifold that separates 'lower' orbits, which decay directly to the laminar state, from 'upper' orbits, which decay more slowly and less directly. The object of this paper is to elucidate the structure of the edge that makes this behaviour possible. To this end we consider a succession of low-dimensional models. In doing this we isolate geometric features that are robust under increase of dimension and are therefore candidates for explaining analogous features in higher dimension. We find that the edge, which is the stable manifold of a 'lower-branch' state, winds endlessly around an 'upper-branch' state in such a way that upper orbits are able to circumnavigate the edge and return to the laminar state.

Key words: bifurcation, low-dimensional models, transition to turbulence

1. Introduction

The Navier–Stokes (NS) equations may be viewed as a dynamical system of infinite dimension. This is a view that has seen some remarkable successes in the problem of turbulence in shear flows (Waleffe 1997; Eckhardt 2008). The latter problem is approached theoretically by considering first a laminar shear flow (plane Couette flow, pipe flow, etc.) and its stability as the Reynolds number R is increased. What distinguishes the problem of shear flow from other hydrodynamic problems, and indeed from many other problems in applied mathematics, is that the onset of the turbulent or disordered state is not accompanied by an instability of the laminar flow. This places particular importance on understanding the nature of the boundary of the basin of attraction of the stable, laminar state and how it changes with R. This boundary is an invariant set and, at least in straightforward examples, is of codimension one. For sufficiently small values of R, the laminar flow is the only steady state and it is globally stable: all perturbations die out (i.e. relaminarize). When R exceeds a critical value R_{SN} additional steady states may appear and it can no longer be strictly true that all perturbations relaminarize. It nevertheless continues to be true that relaminarization is ubiquitous: almost all orbits die out. Exceptions are those lying on a certain codimension-one invariant manifold, called an edge (Duguet, Willis & Kerswell 2008; Vollmer, Schneider & Eckhardt 2009), and separating orbits that die out quickly from orbits that die out slowly. The edge is in many examples

† Email address for correspondence: lebovitz@cs.uchicago.edu

the stable manifold of an 'edge state' which may take one of a number of forms (e.g. an equilibrium point, a periodic orbit, a chaotic saddle, etc.). A pair of relaminarizing orbits may originate extremely close to one another, one just below the edge (a lower orbit) and the other just above (an upper orbit). Orbits on the edge cannot relaminarize as they tend, not to the laminar point, but to the edge state.

Is this edge the basin boundary? There is a convention involved in answering this question. Intuitively a boundary separates one region from another whereas the edge merely separates one part of the basin of attraction from another part of the same region. However, a widely accepted mathematical definition of the boundary ∂S of a set $S \in R^n$ is

> ∂S consists of points $x \in R^n$ such that any neighbourhood of x contains both points that are in S and points that are not in S.

Under this definition edge points are indeed points of the basin boundary, and we adopt this convention here (see also Lebovitz 2012).

The issue addressed in this paper is that of the geometric structure of the edge. This question has been raised before in the specific form: how do upper orbits relaminarize? It arises because familiar pictures of basin boundaries present obstacles to relaminarization (see the discussion in Vollmer *et al.* (2009)). For example, if one envisages the edge as a spherical surface surrounding the laminar point, an upper orbit would have to penetrate this surface to relaminarize, and this is not possible since the surface is an invariant set. If the edge is rather like a plane, it could not be a complete plane separating phase space for the same reason. If the edge of either of these examples is replaced by a subset of itself, it would have a boundary and this would likewise be an invariant set which one should be able to identify in the dynamics. These questions have led to speculations regarding the structure of the edge (Skufca, Yorke & Eckhardt 2006). In the spirit that we are unlikely to understand that structure in the infinite-dimensional case if we do not understand it in the finite-dimensional case, we consider the latter in this paper.

In the context of the low-dimensional models discussed here, we find a consistent picture of the edge and relate it to familiar invariant sets. We study it in a succession of dynamical systems of increasing dimension. The strategy is to isolate properties of the edge that are common to them all since we then have grounds to speculate that these properties generalize to higher, perhaps infinite, dimension.

There are three principal sections, bracketed by preliminaries (§ 2) and a discussion (§ 6) containing a distillation of the detailed information obtained in studying the models of §§ 3–5. In § 3 we recapitulate results previously obtained for a two-dimensional model (Lebovitz 2012) and present a cartoon generalization of it to a three-dimensional model which turns out to contain, in a relatively simple setting, the principal structures of the basin boundary found in the higher-dimensional models. We consider a well-known four-dimensional model of Waleffe in § 4 and investigate the structure of the edge, indicating its extent and complexity. Section 5 is devoted to a six-dimensional model for which the basin boundary has a strong family resemblance to those of the lower-dimensional models despite differences of detail.

2. Preliminaries

Suppose that the shear flow under investigation is described by the velocity field U, and that the NS equations are modified by subtracting U from the total velocity. This has the effect that the unperturbed flow is then represented by the solution $u = 0$

of the modified NS equations. If a fixed set of n basis functions, satisfying the boundary conditions and the condition of incompressibility, is then chosen and used for a Galerkin projection of these modified equations, one finds

$$\frac{\mathrm{d}\boldsymbol{x}}{\mathrm{d}t} = \boldsymbol{A}\boldsymbol{x} + \boldsymbol{b}(\boldsymbol{x}), \quad \boldsymbol{x} \in R^n \tag{2.1}$$

where the ith component x_i of the vector $\boldsymbol{x}$ is the coefficient of the ith basis function. The matrix $\boldsymbol{A}$ and the nonlinear term $\boldsymbol{b}$ inherit features of the full problem. The matrix $\boldsymbol{A}$ is stable (i.e. all of its eigenvalues have negative real parts), and it is non-normal. These conditions taken together imply that, while all solutions of the linearized problem die out (or relaminarize), some of them may undergo a large-amplitude transient before relaminarizing. The amplitude of this transient is found to increase with R. This is a general feature of shear flows (cf. Butler & Farrell 1992). The nonlinear term $\boldsymbol{b}$ is quadratic in $\boldsymbol{x}$, reflecting the quadratic nonlinearity of the NS equations. Moreover, one finds $(\boldsymbol{x}, \boldsymbol{b}(\boldsymbol{x})) = 0$ where $(\cdot, \cdot)$ denotes the inner product, reflecting conservation of energy of the corresponding Euler equations.

In earlier studies (Lebovitz 2009, 2012) emphasis was placed on discovering the emergence of an edge via a homoclinic bifurcation as parameters change. Since in the present paper it is the structure of the edge we wish to study, we restrict consideration to parameter regimes in which the edge is already present.

Much of the description found below depends on relating various invariant sets and manifolds to one another. We use standard notation such as O, X_{lb}, X_{ub} to denote equilibrium points, and B, SM, UM to denote the invariant sets basin of attraction, stable manifold, unstable manifold, respectively. Thus, $B(O)$ is the basin of attraction of the origin, $\partial B(O)$ is its boundary, $SM(X_{lb})$ is the stable manifold of the point X_{lb}, etc.

3. Lowest dimensions

In this section we consider a two-dimensional and a three-dimensional model. Each is of the shear-flow type of (2.1) but no further claim beyond that is made regarding their faithfulness to the shear-flow problem.

3.1. *A two-dimensional model*

We begin with a model introduced by Lebovitz (2012):

$$\dot{x}_1 = -\delta x_1 + x_2 + x_1 x_2 - 3x_2^2, \quad \dot{x}_2 = -\delta x_2 - x_1^2 + 3x_1 x_2, \quad \delta = 1/R. \tag{3.1}$$

We summarize some of its features as studied in Lebovitz (2012).

The critical value below which the origin is globally, asymptotically stable is $R_{SN} = 2$. There a saddle-node bifurcation occurs and for larger values of R there are, in addition to the origin, two further equilibrium points: the lower-branch equilibrium point X_{lb} and the upper-branch equilibrium point X_{ub}. Of these X_{ub} is initially stable whereas X_{lb} is unstable for all $R > R_{SN}$, with a one-dimensional stable manifold and a one-dimensional unstable manifold, indicated by SM and UM in figure 1. The stability properties of X_{ub} change when $R = 2.5$ where a Hopf bifurcation takes place so we consider a smaller value (we use $R = 2.45$ as an example) for which X_{ub} is stable and a larger value (we use $R = 2.55$) for which it is unstable with a complex-conjugate pair of eigenvalues.

The qualitative properties of $\partial B(O)$, the boundary of the basin of attraction of the origin change only slightly under this change of R, and may be described as follows.
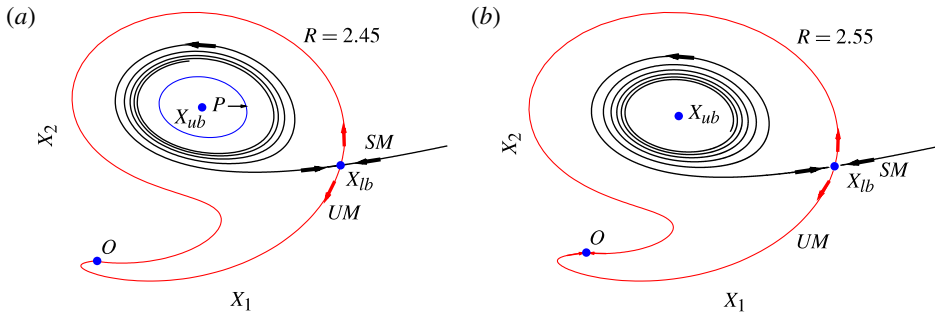
FIGURE 1. (Colour online) In the left-hand figure, the left-hand arc of the stable manifold SM of X_{lb} winds around a periodic orbit P, which is itself the boundary of the basin of attraction of X_{ub}; $\partial B(O)$ is the union of two invariant manifolds, $SM(X_{lb})$ and P. In the right-hand figure X_{ub} is now unstable and $\partial B(O)$ is the union of $SM(X_{lb})$ with the point X_{ub}.

(a) $R = 2.45$: we call attention to $SM(X_{lb})$, the stable manifold of X_{lb}, denoted by SM in figure 1. It consists of two orbits tending to X_{lb} as $t \to \infty$. As $t \to -\infty$, the right-hand orbit is unbounded, whereas the left-hand orbit winds around the periodic orbit P and therefore remains in a bounded region of phase space. It is clear that $\partial B(O)$ is the union of two sets:

$$\partial B(O) = SM(X_{lb}) \cup P. \tag{3.2}$$

The periodic orbit P separates points in $B(O)$ from points in $B(X_{ub})$, the basin of attraction of X_{ub} and therefore clearly forms one part of the boundary of $B(O)$ (called a 'strong' part in Lebovitz (2012)). Here $SM(X_{lb})$ does not separate $B(O)$ from any other set: it merely separates orbits in $B(O)$ with one kind of evolution from orbits in $B(O)$ with a different kind of evolution. Therefore $SM(X_{lb})$ is an edge (or a 'weak' part of the boundary, as defined by Lebovitz (2012)).

Consider the open set bounded by $UM(X_{lb})$ (the outer curves, shown in red online, in figure 1) together with the laminar point O. Modify it by excluding the point X_{ub}. Any orbit beginning at a point in this modified region, when integrated backwards in time, tends to P. Thus, this bounded, two-dimensional region is $UM(P)$. Furthermore, there is one orbit in $UM(P)$ which tends (as $t \to +\infty$) to X_{lb}, i.e. while $UM(P)$ and $SM(X_{lb})$ are not the same, they have a non-trivial intersection consisting of the left-hand arc of $SM(X_{lb})$. This is a bounded orbit and its α-limit set is precisely P.

(b) $R = 2.55$. The stability of X_{ub} ceases at $R = 2.5$ and with it its basin of attraction and the periodic orbit P. Now

$$\partial B(O) = SM(X_{lb}) \cup \{X_{ub}\} \tag{3.3}$$

and consists solely of an edge: all orbits in the plane except those lying on $\partial B(O)$ relaminarize.

The unstable manifold $UM(X_{ub})$ has essentially the same description as that of $UM(P)$ for the case $R = 2.45$ above. Again there is a single orbit, the left-hand arc of $SM(X_{lb})$, representing the intersection $UM(X_{ub}) \cap SM(X_{lb})$. The α-limit set of the left-hand arc of $SM(X_{lb})$ is now the (unstable) equilibrium point X_{ub}.
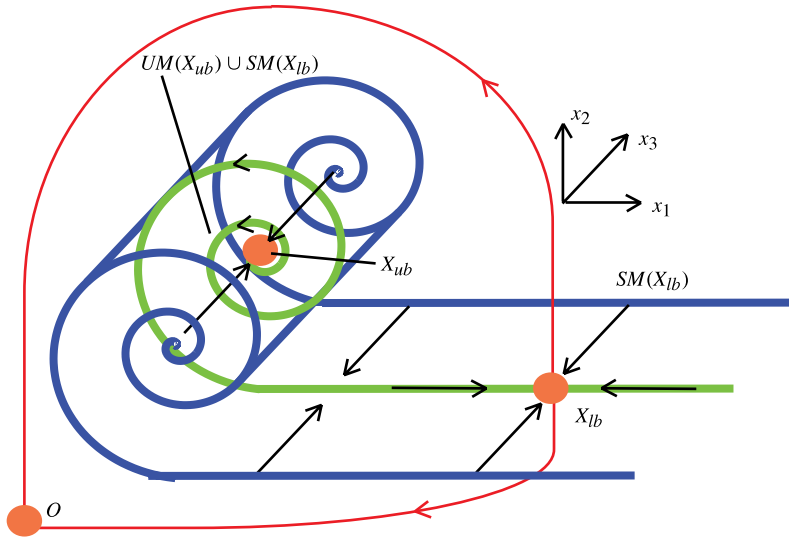
FIGURE 2. (Colour online) The stable manifold $SM(X_{lb})$ is now two-dimensional and forms the edge. The unstable manifold $UM(X_{ub})$ is likewise two-dimensional and has a one-dimensional intersection with $SM(X_{lb})$.

It is clear that orbits beginning on one side of $SM(X_{lb})$ undergo a different evolution from those beginning on the other side. Orbits beginning in the windings around X_{ub} may persist for a long time before relaminarizing.

3.2. *A three-dimensional generalization*

The proceeding discussion provides an understandable model of an edge state, but two-dimensional dynamical systems have special properties which may fail to generalize to higher-dimensional systems. As a first pass at trying to understand what may happen in such generalizations, we augment the system (3.1) with the single equation

$$\dot{x}_3 = -x_3. \tag{3.4}$$

The resulting equations continue to conform to the pattern of (2.1) above. Any of the three equilibrium points (a_1, a_2) of the system (3.1) with (say) $R = 2.55$ becomes an equilibrium point $(a_1, a_2, 0)$ of the three-dimensional model. Building a cartoon on this model, we arrive at the figure 2. Note that if we had considered the case $R = 2.45$ instead, the cartoon diagram would include the periodic orbit P as well, now lying in the plane $x_3 = 0$.

In this figure $SM(X_{ub})$ is now the x_3 axis. The unstable manifold $UM(X_{ub})$ is the same as in the two-dimensional model: it is a bounded, two-dimensional region lying in the x_1x_2 plane, and it intersects $SM(X_{lb})$ along a single curve (the middle curve, shown in green online, in figure 2) The 'folds' of the spiralling orbit of the two-dimensional system have become two-dimensional 'scrolls' parallel to the x_3 axis, and the flow through a generic point near X_{ub} is now trapped for a time within these scrolls, ultimately relaminarizing. The same general picture holds in the case $R = 2.45$ except that the scrolls wind up, not on a straight line through X_{ub} but on the cylinder parallel to the x_3 axis and containing the periodic orbit P. The stable manifold of P is bounded by this cylinder; it forms the boundary of the basin of attraction of X_{ub}.

In both the two- and three-dimensional models, most orbits do not get particularly close to X_{lb}: only those beginning very close to $SM(X_{lb})$ do that. Two points very near a fold (or scroll) of $SM(X_{lb})$ but on opposite sides of it pass close to X_{lb} but must continue to lie on opposite sides of $SM(X_{lb})$, and therefore have final evolutions toward O that are quite different. Moreover, orbits that begin between inner folds (or scrolls) must first wind their way out before approaching X_{lb} and may for this reason have very long lifetimes.

We pass on now to a model adhering more closely to the fluid dynamics.

4. Waleffe's four-dimensional model

The four-dimensional model proposed in Waleffe (1997) (hereafter referred to as W97) adheres closer to the shear-flow problem in that its derivation is guided by Galerkin projection onto modes believed to be decisive for the nonlinear development of (in this case) plane Couette flow. When shifted so as to make the origin of coordinates correspond to the unperturbed, laminar state, W97 takes the form

$$\dot{x}_1 = -\delta r_1 x_1 - \sigma_2 x_2 x_3 + \sigma_1 x_4^2, \tag{4.1a}$$

$$\dot{x}_2 = -\delta r_2 x_2 + \sigma_2 x_3 + \sigma_2 x_1 x_3 - \sigma_4 x_4^2, \tag{4.1b}$$

$$\dot{x}_3 = -\delta r_3 x_3 + \sigma_3 x_4^2, \tag{4.1c}$$

$$\dot{x}_4 = -\left(\sigma_1 + \delta r_4\right) x_4 + x_4 \left(\sigma_4 x_2 - \sigma_3 x_3 - \sigma_1 x_1\right). \tag{4.1d}$$

Here $\delta = 1/R$ represents the reciprocal of the Reynolds number, whereas the coefficients $\sigma_i, r_i, i = 1, \ldots, 4$ are positive numbers derived via Waleffe's Galerkin procedure. In this paper the values of the σ and the r are taken to be

$$(\sigma_1, \sigma_2, \sigma_3, \sigma_4) = (0.31, 1.29, 0.22, 0.68), \tag{4.2a}$$

$$(r_1, r_2, r_3, r_4) = (2.4649, 5.1984, 7.6729, 7.1289). \tag{4.2b}$$

They correspond (approximately) to the wavenumber values

$$\alpha = 1.30, \quad \gamma = 2.28. \tag{4.3}$$

These are (approximately) the values adopted in other studies of this system such as those of Dauchot & Vioujard (2000) (where slight numerical discrepancies from those found here are attributable to correspondingly small differences adopted for these parameters) and Cossu (2005).

The system (4.1) possesses the symmetry $S = \mathrm{diag}(1, 1, 1, -1)$. The hyperplane $x_4 = 0$ is therefore an invariant plane. It is not difficult to show that this plane lies in the basin of attraction of the origin. Since orbits cannot cross it, any structure made up of orbits, such as other invariant sets, lie in one or another of the two regions $x_4 > 0$ and $x_4 < 0$. We confine our attention to the region $x_4 > 0$, bearing in mind that any structures we find there are duplicated in the region $x_4 < 0$.

4.1. *Equilibrium points*

The origin of coordinates is an asymptotically stable equilibrium point and therefore has a basin of attraction $B = B(O)$.

The transition from the purely laminar toward more complicated behaviour is governed by the existence and the structure of the boundary of B. These are intimately connected with X_{lb} and X_{ub}, the lower- and upper-branch equilibrium points (figure 3) and we now turn to an examination of these.
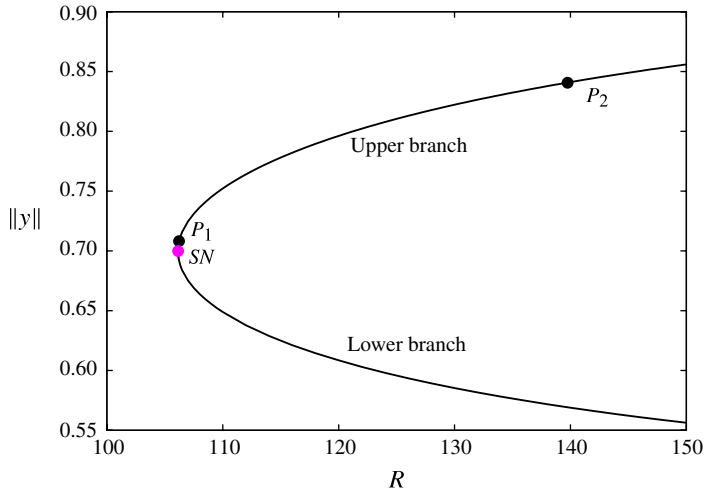
FIGURE 3. (Colour online) The diagram of the norms of equilibrium solutions against the Reynolds number R. For the chosen values of parameters in W97 there is a saddle-node bifurcation at $R_{SN} = 106.1393$. Changes in the eigenvalues at the upper branch equilibrium point occur as indicated in the text, at the values $R_{P_1} = 106.2401$ and $R_{P_2} = 139.73738$. The laminar solution $\|y\| = 0$ (not shown) is stable for all values of R.

4.1.1. *The lower branch*

This branch of equilibrium points has uniform stability properties: one unstable and three stable eigenvalues for all values of $R > R_{SN}$. There is accordingly a three-dimensional stable manifold $SM(X_{lb})$ and a one-dimensional unstable manifold $UM(X_{lb})$. As discussed more fully below (§ 4.2), $SM(X_{lb})$ is the edge and the two arcs of $UM(X_{lb})$ both lead, via different paths, to O.

4.1.2. *The upper branch*

This branch undergoes a change in its stability properties at P_2. From the outset at SN to the nearby point P_1, it is unstable with a complex pair of eigenvalues with negative real part and two real, positive eigenvalues. It remains unstable at P_1 but the positive real roots coalesce and become a complex pair with a positive real part. At P_2 this positive real part passes through zero and, for larger values of R, is negative. The upper branch therefore becomes and remains stable for $R > R_{P_2}$.

The bifurcation at P_2 is of the Hopf type and is therefore accompanied by the birth of a periodic orbit P. This orbit would be stable if it existed for $R < R_{P_2}$, but it appears (on numerical evidence) that the new periodic orbit exists for $R > R_{P_2}$ and is therefore unstable. Since each upper-branch equilibrium point X_{ub} is asymptotically stable if $R > R_{P_2}$, X_{ub} has its own basin of attraction, which we will call $D = B(X_{ub})$ to distinguish it from the principal object of study $B = B(O)$. We have numerical evidence that the unstable periodic orbit P lies on ∂D and, in fact, that the stable manifold of P coincides with ∂D.

The structure of solutions near X_{ub} is important for understanding the edge because it is the winding up of the latter around X_{ub} (for $R < R_{P_2}$) or around $D = B(X_{ub})$ (for $R > R_{P_2}$) that allows orbits from both sides of the edge to relaminarize.
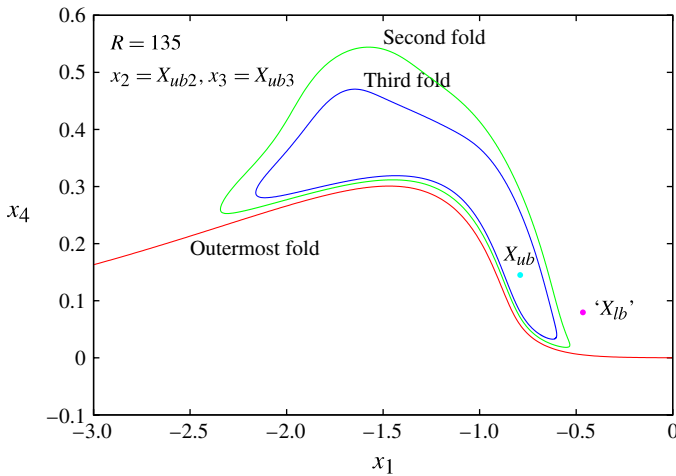
FIGURE 4. (Colour online) The stable manifold of X_{lb} winds around X_{ub} infinitely often, producing a succession of three-dimensional folds. In this slice (the x_4–x_1 slice passing through X_{ub}) the outermost fold appears to be unbounded both to the left and the right (the other folds are bounded and appear as closed curves in this view). Single quotes around X_{lb} indicate that the latter fails to lie in the chosen hyperplane but is projected onto it.

4.2. *The structure of ∂B*

We first observe the edge character of the stable manifold of X_{lb} by checking the orbits beginning 'just above' and 'just below' X_{lb} for some values of R. By 'just above' we will mean initial values of x for which x_4 is slightly greater than X_{lb4}, and by 'just below' initial values of x for which x_4 is slightly smaller than X_{lb4}, whereas $x_i = X_{lbi}$ for $i = 1, 2, 3$ in both cases. Starting for values of R just greater than R_{SN}, we find that all orbits, whether starting above or below, relaminarize. Those starting above take longer. We have done this for a large number of values of R, up to $R = 10\,000$, and find that this holds without exception.

We next construct parts of $SM(X_{lb})$ by a continuation method, starting at $x = X_{lb}$. The parts that are constructed are the intersections of $SM(X_{lb})$ with various hyperplanes, as indicated in the figures. In these figures, in order to emphasize the nature of $SM(X_{lb})$ near the other equilibrium point X_{ub}, the hyperplanes are chosen to pass through this point.

Whereas $SM(X_{lb})$ cannot, by definition, belong to B, it can and does belong to ∂B. Indeed, it seems that $SM(X_{lb}) = \partial B$ for some values of R. This is so for $R < R_{P_2} \approx 139.7$ and we investigate an example of this ($R = 135$) first.

4.2.1. *R=135*

In this case ∂B consists of the union of $SM(X_{lb})$ with the single point X_{ub}. The intersection of this set with the hyperplane $x_2 = X_{ub2}, x_3 = X_{ub3}$ is shown in figure 4.

Points on any of these folds tend, under the flow, toward X_{lb} as $t \to \infty$. For example, a point starting on the third fold, after making two loops about X_{ub}, then tends toward X_{lb}. Higher-order folds (not shown) get arbitrarily close to X_{ub}, and orbits originating on them make more loops (and require more time), before tending toward X_{lb}. A point very close to a fold, but not exactly on it, will generate an orbit coming very close to X_{lb}, but will then tend to O along one of the arcs of $UM(X_{lb})$: its final descent to O
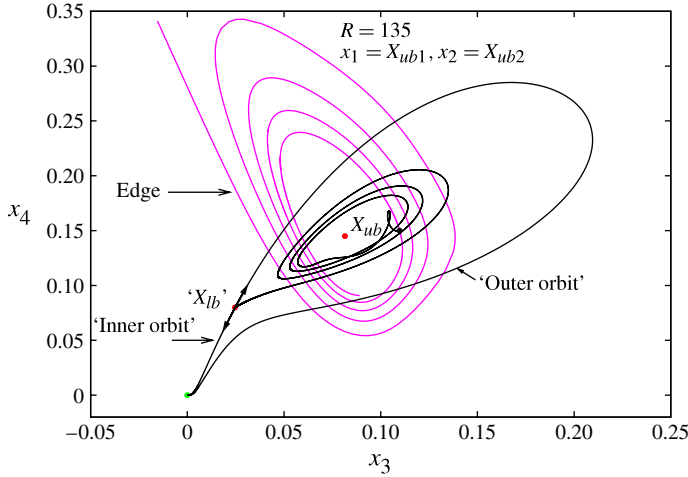
FIGURE 5. (Colour online) A slice (marked 'edge') is shown as in figure 4 but now in the $x_3 x_4$ plane. It is bounded in the $+x_3$ direction. Projections of two orbits are also shown: they start, one on either side of the fourth fold of the edge, very near the black dot on the edge and illustrate the behaviour of such orbits as described in the text. The orbits are indistinguishable until they approach X_{lb}. They linger there for a long time before tending toward O along the two, opposite, unstable directions of X_{lb}.

will therefore depend on which side of the fold it originated from. The similarity with the two-dimensional case (figure 1, $R = 2.55$) is clear.

However, the outermost fold of figure 4 appears to extend indefinitely in the $\pm x_1$ directions whereas, in order for the picture of an edge obtained from the two-dimensional model to persist, there must be lines in phase space along which all folds are bounded at least on one side. We therefore investigate a second slice through X_{ub} but in a different hyperplane (figure 5). Here we find indeed that $SM(X_{lb})$ is bounded in the $+x_3$ direction.

We next investigate the case when $R = 145 > R_{P_2}$.

4.2.2. $R = 145$

For values of $R > R_{P_2}$ the point X_{ub} is stable. We consider its basin of attraction D and its boundary ∂D. In this case ∂B is the union of two sets: a weak boundary component ($SM(X_{lb})$, the edge) and a strong boundary component (∂D), shown in figure 6. Consider ∂D first.

The Hopf bifurcation at $R \approx 139.7$ results in a periodic orbit P for larger values of R. For the current value, $R = 145$, P is found to have period $T = 140.69$ and Floquet exponents with magnitudes

$$|\lambda| = 1.000, 1.2003, 0.5359 \times 10^{-3} \quad \text{(multiplicity 2)}. \quad (4.4)$$

Thus, it is unstable with a three-dimensional stable manifold, $SM(P)$; nearby orbits on its stable manifold are drawn toward it very rapidly. We find numerically that P lies on ∂D and indeed that orbits originating on ∂D are all attracted toward P, and we conclude from this that $\partial D = SM(P)$.

We now consider the edge, the weak component of ∂B. It is $SM(X_{lb})$ and we seek a slice through it by the hyperplane $x_2 = X_{ub2}, x_3 = X_{ub3}$.
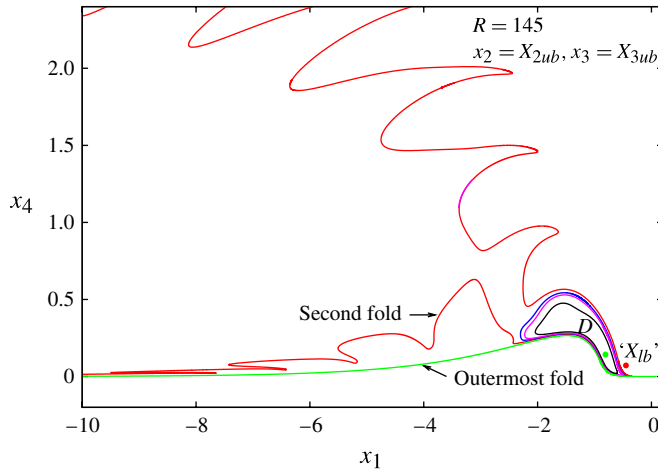
FIGURE 6. (Colour online) The point X_{ub} (shown as a green dot online) is now stable and the $x_1 x_4$ slice through its basin of attraction D is shown. The outermost fold of the edge (shown in green online) extends a great distance into phase space and may not terminate, the second fold terminates on the right but not the left and the inner windings intersect this slice as finite closed curves.

This is also shown in figure 6. The first, or outermost, fold of the edge (shown in green online) appears to cover the x_1 axis: we surmise that, as in the case $R = 135$, this would not be so along the x_3 axis. The second fold (shown in red online) is highly convoluted and appears to cover the negative, but not the positive, x_1 axis. Subsequent folds are finite closed curves that conform their shape to that of the indicated slice of $D = B(X_{ub})$.

The general similarity of these folds to those of the preceding case ($R = 135$) are clear and the general features of the edge allowing all orbits to relaminarize would likewise appear similar. The main difference is that there is now (i.e. for $R = 145$) a region of phase space (D) where orbits are permanently trapped and unable to relaminarize.

5. A six-dimensional model

We consider finally a six-dimensional system modelling plane Poiseuille flow via a procedure similar to that used in Waleffe (1997) to model plane Couette flow. The Galerkin basis functions onto which the NS equations are projected are discussed and presented in some detail in Mariotti (2011). The resulting system, again shifted so that the origin O represents the unperturbed, laminar flow, has the canonical structure (2.1) where

$$A = \begin{bmatrix} -k_1 & 0 & 0 & 0 & 0 & 0 \\ 0 & -k_2 & \sigma_0 & 0 & 0 & 0 \\ 0 & 0 & -k_3 & 0 & 0 & 0 \\ 0 & 0 & 0 & -k_4 & 0 & -\sigma_3 \\ 0 & 0 & 0 & 0 & -k_5 & 0 \\ 0 & 0 & 0 & \sigma_3 & 0 & -k_6 \end{bmatrix} \qquad (5.1)$$

and

$$\boldsymbol{b} = \begin{bmatrix} -\sigma_0 x_2 x_3 \\ \sigma_0 x_1 x_3 - \sigma_1 x_4 x_5 \\ -(\sigma_4 + \sigma_5) x_5 x_6 \\ \sigma_2 x_2 x_5 - \sigma_3 x_1 x_6 \\ (\sigma_1 - \sigma_2) x_2 x_4 + (\sigma_4 - \sigma_6) x_3 x_6 \\ (\sigma_5 + \sigma_6) x_3 x_5 + \sigma_3 x_1 x_4 \end{bmatrix}. \tag{5.2}$$

The constants $k_i, \sigma_i, \ i = 1-6$ are all functions of wavenumbers α, β, γ in the x, y, z directions, respectively. The formulas determining them may be found in Mariotti (2011). Here we note only that k_i is positive for each $i = 1-6$, confirming the (expected) stability of the laminar solution. For the purposes of the numerical calculations of the present section, the values of the wavenumbers are taken to be

$$\alpha = 1.1, \quad \beta = \pi/2, \quad \gamma = 5/3. \tag{5.3}$$

The system (2.1) with the choices of $A, b(x)$ indicated above is easily found to possess the group (of order four) of symmetries generated by

$$S_1 = \text{diag}(1, 1, 1, -1, -1, -1) \quad \text{and} \quad S_2 = \text{diag}(1, -1, -1, 1, -1, 1). \tag{5.4}$$

The hyperplane $x_4 = x_5 = x_6 = 0$ is invariant and lies in the basin of attraction of the origin.

5.1. *Periodic orbits*

A search for equilibrium points failed. It included reduction to an eighth-order polynomial in x_5, a Gröbner-basis reduction using Matlab and a search for equilibria asymptotically for large R. On the other hand, a search for a stable, periodic orbit, in a region of phase space suggested by the linearly optimal direction for the system $\dot{x} = Ax$, was successful. Having found one such orbit for a particular value of R (we used $R = 500$), one can follow it as R changes using continuation software (we used MatCont: cf. Dhooge, Govaerts & Kuznetsov (2003)). The result is a pattern very similar to that seen in the preceding examples, with the difference that periodic orbits (*PO*) play the roles previously played by equilibrium points. Such orbits exist for all values of $R > R_{SN} \approx 291.7$. For the symmetry $S_3 = S_1 S_2$ they satisfy the condition $S_3 x(t) = x(t + T/2)$ where T is the period. From this one infers that the average values of x_2, x_3, x_4 and x_6 all vanish for these orbits.

5.2. *Bifurcations*

The bifurcation and stability patterns of the family of periodic orbits depicted in figure 7 are analogous to those of W97.

The lower-branch periodic orbits, PO_{lb}, are unstable for all values of $R > R_{SN} \approx 291.7$ with a single Floquet multiplier of magnitude exceeding unity (cf. figure 7b). Thus, $SM(PO_{lb})$ has dimension five (codimension one).

The upper-branch orbits, on the other hand, undergo stability changes. For values of R barely exceeding R_{SN} the pair of Floquet multipliers of unstable type are real but, at the nearby value $R_{P_1} \approx 292.4$, they coalesce and become a complex-conjugate pair, still of unstable type (cf. figure 7c). The stability of this pair changes at a third critical value $R_{P_2} \approx 305.5$ and for larger values of R the upper-branch periodic orbit is stable. Thus, for $R > R_{P_2} PO_{ub}$ possesses its own basin of attraction $B(PO_{ub})$.
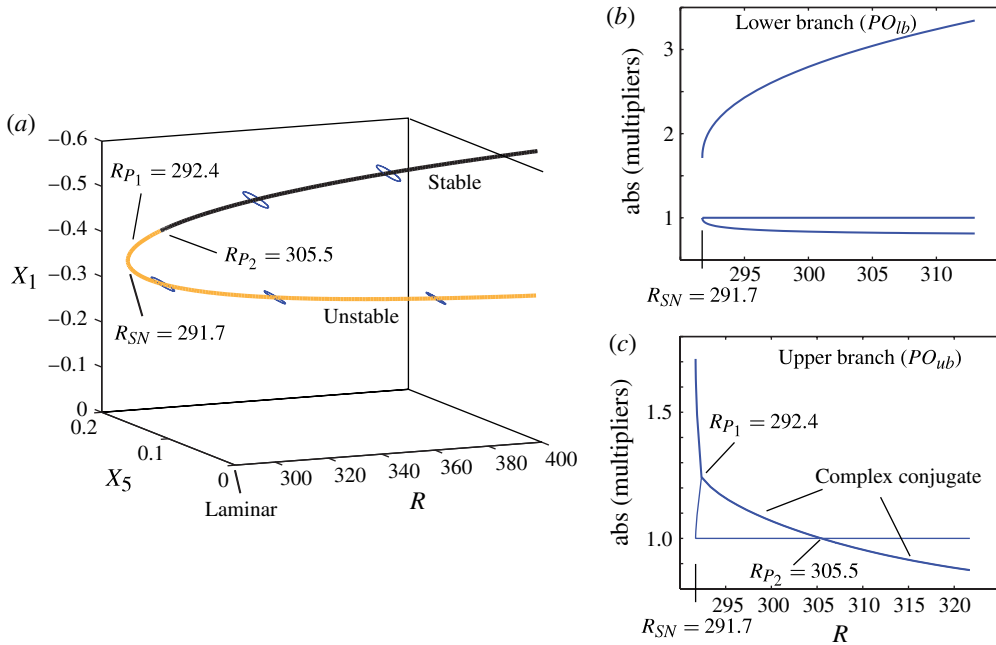
FIGURE 7. (Colour online) (*a*) Projections of periodic orbits: the curve represents the positions of the centres in the x_1–x_5 plane against R. The averaged values of coordinates x_2, x_3, x_4, x_6 on these orbits all vanish. (*b*,*c*) Magnitudes of the three greatest Floquet multipliers.

The bifurcation at $R = R_{P_2}$ is of Neimark–Sacker type and results, for $R > R_{P_2}$, in the creation of an invariant torus. This torus has dimension five and forms the boundary of the basin of attraction of PO_{ub}, and hence plays a role analogous to ∂D, the boundary of the basin of attraction of X_{ub}, in W97.

5.3. *The structure of the edge*

We first consider the case with $R > R_{P_2}$. As in the preceding examples, we use a continuation method to identify the intersection of $SM(PO_{lb})$ with the hyperplane x_1–x_5. Also in this case $SM(PO_{lb})$ has the characteristic of an edge: initial conditions arbitrarily close but on different sides of $SM(PO_{lb})$ have qualitatively different trajectories (see for example figure 8*b*, trajectories p_4 and p_5).

We found evidence that the edge is wrapped around $B(PO_{ub})$, as indicated by the fold shown in figure 8. The structure of the edge is clarified by considering a transect of initial conditions crossing $\partial B(PO_{ub})$ (figure 9). Moving the initial conditions along the transect, we find that trajectories belonging to $B(O)$ are characterized by discrete steps in relaminarization time. These steps are associated to successive loops of the trajectory around the torus orbit before it decays to the origin, i.e. every fold of $SM(PO_{lb})$ determines a band of increasing relaminarization time (figure 9). Along the transect direction toward $\partial B(PO_{ub})$, the distance between two consecutive steps in relaminarization becomes smaller, suggesting that the edge folds infinitely many times around $\partial B(PO_{ub})$. As a result, trajectories starting in $B(O)$ but very close to $\partial B(PO_{ub})$ experience a convoluted relaminarization path (see trajectory p_6 and p_7 in figure 8*c*, and the cartoon in figure 9*b*).
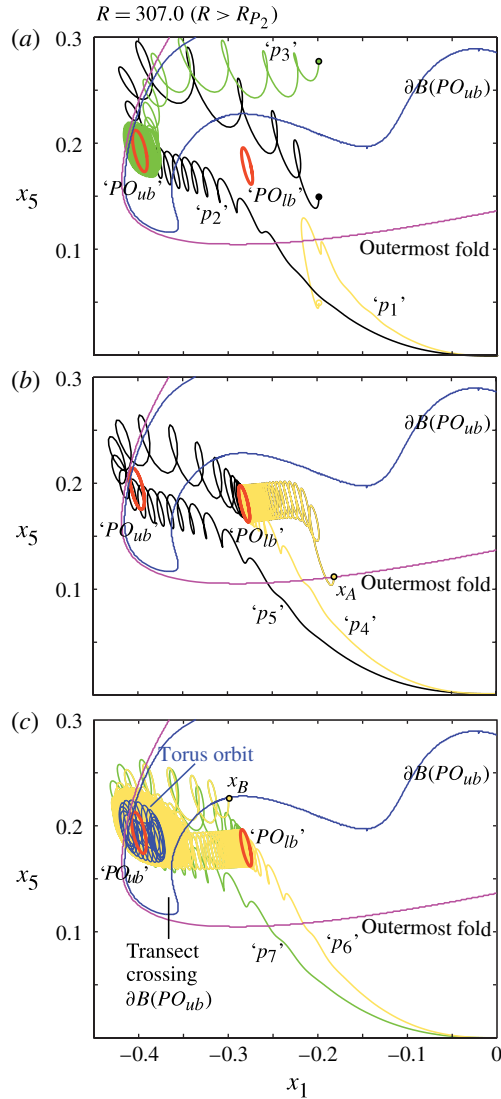
FIGURE 8. (Colour online) Orbits for $R = 307 > R_{P_2}$, for which PO_{ub} is stable (cf. figure 7). Upper- and lower-branch periodic orbits are projected onto the x_1–x_5 plane. The other initial conditions are fixed at $(x_2, x_3, x_4, x_6) = (-0.0511, -0.0391, 0.0016, 0.1260)$, which correspond to a point on PO_{ub}. (*a*) The trajectory p_1 lies well on one side of $SM(PO_{lb})$ and relaminarizes quickly and directly, p_2 well on the other side and relaminarizes less quickly and only after visiting a neighbourhood of PO_{ub}; p_3 lies in $B(PO_{ub})$. (*b*) Here x_A lies on $SM(PO_{lb})$. One orbit (p_4) starts very near to x_A on one side of $SM(PO_{lb})$, is attracted toward PO_{lb}, lingers for a while and then decays. A second orbit (p_5) starts very near to x_A on the other side, follows essentially the same (shown in yellow online) path toward PO_{lb}, lingers a while, but then has a different kind of decay (black): it first visits a neighbourhood of PO_{ub}. (*c*) Here x_B lies on $SM(PO_{lb})$, but on an inner fold and close to the torus $\partial B(PO_{ub})$. As a result, two orbits starting close to x_B, p_6 and p_7, experience a long and convoluted path around the torus (blue). Both trajectories then approach PO_{lb} before eventually relaminarizing. Then p_6 (the lower orbit, shown in yellow online) decays immediately whereas p_7 (the upper orbit, shown in green online) first revisits a neighbourhood of the torus and only then decays.
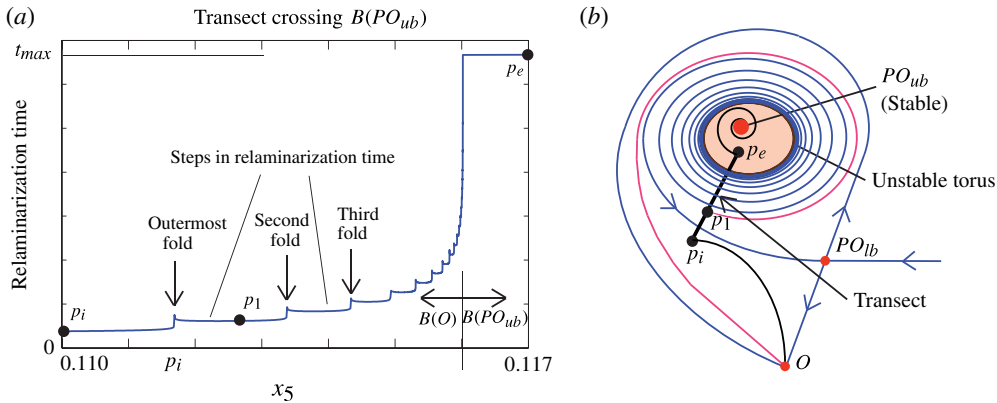
FIGURE 9. (Colour online) (*a*) Analysis of a transect of initial conditions crossing $\partial B(PO_{ub})$, for $R = 307 > R_{P_2}$ (cf. figure 8*c*). The transect is aligned along the direction X_5, keeping all of the other initial conditions fixed. The first point, p_i, corresponds to a trajectory that relaminarizes 'directly', while the last point, p_e, corresponds to a trajectory that converges to PO_{ub}. The step-wise increase in relaminarziation time is associated with crossing folds on the edge. (*b*) Cartoon of the phase space, with the laminar fixed point, PO_{ub}, PO_{lb}, the torus orbits and a trajectory as an example, explaining the steps in relaminarization time associated with crossing folds on the edge.

A similar edge behaviour is found for $R_{P_1} < R < R_{P_2}$, with the difference that $B(PO_{ub})$ collapses to PO_{ub}. Hence, our numerical explorations suggest the presence of an edge structure for $R > R_{P_1}$.

The emergent picture is consistent with the interpretation that, for a range of R values ($R > R_{P_2} \approx 305.5$), $\partial B(O)$ consists of the union of a weak part, or edge ($SM(PO_{lb})$), with a strong part ($\partial B(PO_{ub})$). Analogously, for values $R_{P_1} < R < R_{P_2}$, $\partial B(O)$ consists only of the edge together with the single orbit PO_{ub}.

6. Discussion

The most general conclusion that we draw from the preceding calculations is that one can understand ubiquitous relaminarization in terms of the relations of invariant manifolds in finite-dimensional systems of the form (2.1), as described in detail below (§ 6.1). Our picture of the edge appears to be a consistent one, occurring in several models of successively higher dimension. However, consistency is not the same as truth, and there is a lot more to be discovered in this subject. For example, in pipe flow there are multiple lower-branch states (Duguet *et al.* 2008), apparently all lying on a single edge, and there are also multiple upper-branch states. Moreover, the models considered here describe temporal behaviour, whereas the full problem includes spatiotemporal behaviours. Even if the picture presented here continues to provide a building block for ubiquitous relaminarization, a more complete description of the edge and its relations to upper-branch states awaits further study.

In both the four-dimensional model of § 4 and the six-dimensional model of § 5 there is an interval of Reynolds number for which the boundary of the basin of attraction of the laminar state ($\partial B(O)$) consists solely of the edge. For larger values of R the upper-branch state (X_{ub} or PO_{ub}) becomes stable and $\partial B(O)$ is the union of the edge with the basin boundary of the newly stable state. It is tempting to see a parallel here with the Reynolds-number behaviour of actual shear flows

(Avila *et al.* 2011; Mullin 2011): for a range of R the turbulence is transient, but beyond a critical value there is (or may be) a turbulent attractor. On the other hand this parallel may be a spurious artifact of the extreme truncation. An understanding of how transient turbulence becomes persistent turbulence is a subject of current research. Some of this concentrates on the nature of upper-branch states (Clever & Busse 1992, 1997; Kreilos & Eckhardt 2012) as does the present paper. In particular, the work of Kreilos & Eckhardt (2012) features not one or a small number of periodic orbits but a period-doubling cascade followed by the onset of chaos.

We briefly recapitulate the nature of the edge structure, and summarize the technique for producing the diagrams of this paper.

6.1. *The edge*

The picture of the edge obtained from the models we have considered is a codimension-one invariant manifold unbounded in some directions in phase space but, importantly, bounded in other directions at least from one side. It is the latter circumstance that enables a pair of orbits originating on opposite sides of this manifold both to tend toward the stable, laminar point as $t \to \infty$. In the cases considered here the edge is a very regular object which coincides with the stable manifold of either an equilibrium point X_{lb} or a periodic orbit PO_{lb}: the 'edge state'. In the work of Skufca *et al.* (2006), for R less than a critical value R_c their edge state was a periodic orbit, and the edge was likewise quite regular. For $R > R_c$ the edge state was a chaotic saddle. However, the edge itself remained regular. We therefore have some reason for hoping that our characterization of the edge will continue to have meaning in some of these 'wilder' cases.

This manifold cannot 'end in thin air' and the claim that it is finite in some directions in phase space requires explanation. This explanation is found, in the present paper, in its relation to a second state, the upper-branch equilibrium point X_{ub} (or the upper-branch periodic orbit PO_{ub}). It is found that the edge winds around the latter state infinitely often, never quite touching. Since the stable manifold of the edge state is of codimension one, orbits starting near the edge but on opposite sides of it tend to be entrained by its one-dimensional unstable manifold. When the edge state is an equilibrium point, the unstable manifold consists of a pair of arcs, each of which tends to the laminar point as $t \to \infty$. The entrained orbits tend to the origin, although they follow quite different evolutions depending on the side of the edge from which they originated. A similar picture is found when the edge state is a periodic orbit, except that now the unstable manifold is two-dimensional.

The nature of an orbit and the time for its relaminarization depend on whether the starting point of the orbit lies above the edge, in which case it must circumnavigate the upper-branch state and its associated invariant manifolds, or below the edge, in which case it has a more direct route to relaminarization. However, there are two further contingencies that may contribute to the relaminarization time of an orbit. One is proximity to the edge: the closer it is to the edge the longer it will linger near the edge state before relaminarizing. The second is related to the fold structure of the edge near the upper-branch state: an orbit that starts between two inner folds is trapped within the fold structure until it winds its way out.

6.2. *Technique*

The computational technique for finding slices of the boundary of the basin of attraction of the lower-branch states found in § 4 of this paper is straightforward. We start with a point known to lie on that boundary. For example, in figure 4, the

point X_{lb} is such a point. Alternatively, we may start with a pair of points of which one relaminarizes quickly (an 'inside' point) and one slowly (an 'outside' point) and produce, by bisection, such a pair that lie extremely close to one another, and which therefore straddle the edge. We slightly alter one of their coordinates (x_1 say) and repeat this procedure so as to find a new pair of points straddling the edge. Once a point in R^n lying on the edge has been located, we can move around in any direction in R^n seeking more edge points in this way.

An alternative method is to locate and record edge points via the transect method described in § 5. A lifetime landscape map (e.g. Skufca *et al.* 2006) is first constructed to isolate the general locations of the edge folds. Then, refined transects across the folds are used to identify discrete steps in relaminarization time (e.g. figure 9*a*), which are associated with increasing loops of the trajectory around the upper-branch state.

Acknowledgements

REFERENCES

AVILA, D., MOXEY, D., DE LOZAR, A., AVILA, M., BARKLEY, D. & HOF, B. 2011 The onset of turbulence in pipe flow. *Science* **333**, 192–196.

BUTLER, K. M. & FARRELL, B. F. 1992 Three-dimensional optimal disturbances in viscous flows. *Phys. Fluids* A **12**, 1637–1650.

CLEVER, R. M. & BUSSE, F. H. 1992 Three-dimensional convection in a horizontal fluid layer subjected to constant shear. *J. Fluid Mech.* **234**, 511–527.

CLEVER, R. M. & BUSSE, F. H. 1997 Tertiary and quaternary solutions for plane couette flow. *J. Fluid Mech.* **344**, 137–153.

COSSU, C. 2005 An optimality condition on the minimum energy threshold in subcritical instabilities. *C. R. Mecanique* **333**, 331–336.

DAUCHOT, O. & VIOUJARD, N. 2000 Phase space analysis of a dynamical model for the subcritical transition to turbulence in plane couette flow. *Eur. Phys. J.* B **14**, 377–381.

DHOOGE, A., GOVAERTS, W. & KUZNETSOV, YU. A. 2003 Matcont: a Matlab package for numerical bifurcation analysis of odes. *ACM Trans. Math. Software* **29**, 141–164.

DUGUET, Y., WILLIS, A. P. & KERSWELL, R. 2008 Transition in pipe flow: the saddle structure on the boundary of turbulence. *J. Fluid Mech.* **613**, 255–274.

ECKHARDT, B. 2008 Turbulence transition in pipe flow: some open questions. *Nonlinearity* **21**, T1–T11.

KREILOS, T. & ECKHARDT, B. 2012 Periodic orbits near the onset of chaos in plane couette flow. http://arxiv.org/abs/1205.0347.

LEBOVITZ, N. 2009 Shear-flow transition: the basin boundary. *Nonlinearity* **22**, 2645–2655.

LEBOVITZ, N. 2012 Boundary collapse in models of shear-flow transition. *Commun. Nonlin. Sci. Numer. Sim.* **17**, 2095–2100.

MARIOTTI, G. 2011 A low dimensional model for shear turbulence in plane poiseuille flow: an example to understand the edge. In *Proceedings of the Program in Geophysical Fluid Dynamics*. Woods Hole Oceanographic Institution.

MULLIN, T. 2011 Experimental studies of transition to turbulence in a pipe. *Annu. Rev. Fluid. Mech.* **43**, 1–24.

SKUFCA, J. D., YORKE, J. A. & ECKHARDT, B. 2006 Edge of chaos in a parallel shear flow. *Phys. Rev. Lett.* **96**, 174101.

VOLLMER, J., SCHNEIDER, T. M. & ECKHARDT, B. 2009 Basin boundary, edge of chaos and edge state in a two-dimensional model. *New J. Phys.* **11**, 013040.

WALEFFE, F. 1997 On a self-sustaining process in shear flows. *Phys. Fluids* **9** (4), 883–900.